Novel Materials and Device Design by Metal-Organic Chemical Vapor Deposition for Use in Infrared Emitters*

R. M. Biefeld, S. R. Kurtz, and A. A. Allerman
Sandia National Laboratory, Albuquerque, NM 87185-0601

Abstract

We have grown AlSb and $AlAs_xSb_{1-x}$ epitaxial layers by metal-organic chemical vapor deposition (MOCVD) using trimethylamine or ethyldimethylamine alane, triethylantimony and arsine. These layers were successfully doped p- or n-type using diethylzinc or tetraethyltin, respectively. We examined the growth of $AlAs_xSb_{1-x}$ using temperatures of 500 to 600 °C, pressures of 65 to 630 torr, V/III ratios of 1-17, and growth rates of 0.3 to 2.7 μm/hour in a horizontal quartz reactor. We have also grown gain-guided, injection lasers using AlAsSb for optical confinement and a strained InAsSb/InAs multi-quantum well active region using MOCVD. The semi-metal properties of a p-GaAsSb/ n-InAs heterojunction were utilized as a source for injection of electrons into the active region of the laser. In pulsed mode, the laser operated up to 210 K with an emission wavelength of 3.8-3.9 μm. The dependence of active region composition on wavelength was determined. We also report on the 2-color emission of a light-emitting diode with two different active regions to demonstrate multi-stage operation of these devices.

DISCLAIMER

Introduction

We are developing mid-infrared (3-6 μm) lasers and LED's for use in chemical sensor systems and infrared countermeasures. As-rich, InAsSb heterostructures display unique electronic properties that are beneficial to the performance of these midwave infrared emitters. We have previously demonstrated an electrically injected, 3.5 μm laser with a strained and nominally "dislocation free," active region [1]. The laser was grown by metal-organic chemical vapor deposition (MOCVD). The active region consisted of 10, biaxially compressed quantum wells of $InAs_{0.94}Sb_{0.06}$. InPSb cladding layers were used for optical confinement. To improve the operating characteristics of our lasers we are exploring the synthesis of Al(As)Sb by MOCVD as confinement layers for these devices. AlSb and $AlAs_xSb_{1-x}$ are of interest for their potential application as optical and electronic confinement layers in a variety of optoelectronic devices such as infrared detectors, resonant tunneling diodes, and laser diodes[1-4]. We are exploring the synthesis of these materials by metal-organic chemical vapor deposition (MOCVD) for their use in 3-6 μm, mid-infrared optoelectronic heterojunction devices.

Although devices using $AlAs_xSb_{1-x}$ have been successfully prepared by molecular beam expitaxy [2,3], there have been no reports to date of their successful use in devices when prepared by MOCVD. We are aware of two previous reports of the successful growth of $AlAs_xSb_{1-x}$ by MOCVD [4,5]. In one of those reports [5], no mention was made of the electrical quality or the impurity level of the materials. Although there have been several reports by others of the growth of AlSb and AlGaSb by MOCVD [5-11], only references [10] and [11] comment on impurity levels. It is well known that Al containing materials prepared using MOCVD tend to have larger concentrations of both O and C impurities when compared to the Ga containing analogues [4,10-14]. The presence of these impurities in Al containing semiconductors is due to the strength of the bond between Al and O or C when compared to the bond strength of Al to P, As, or Sb [12-14]. In our previous work we used trimethylamine alane (TMAA) or ethyldimethylamine alane (EDMAA) and

triethylantimony (TESb) to prepare high quality $AlAs_xSb_{1-x}$ by MOCVD [4] . In this paper we will describe further advances in the preparation of epitaxial layers of n- and p-type $AlAs_xSb_{1-x}$ and the growth of InAsSb/InAs multiple quantum well active region lasers using $AlAs_xSb_{1-x}$ optical confinement layers.

Experimental

This work was carried out in a previously described horizontal MOCVD system [14]. TMAA, or EDMAA, TESb and 100% arsine were the sources for Al, Sb, and As respectively. TEGa, arsine, and TESb were used to grow a 1000 to 2500Å GaAsSb caps on all samples to keep the $AlAs_xSb_{1-x}$ layer from oxidizing. Hydrogen was used as the carrier gas at a total flow of 8 slpm. P-type doping was accomplished using 200 sccm to 500 sccm of diethylzinc (DEZn) diluted to 400 ppm in hydrogen. N-type doping was accomplished using tetraethyltin (TESn) held at 18 ° C to 20 ° C. The hydrogen flow through the TESn source was typically 20 sccm which was diluted with 350 sccm of hydrogen. Five to 20 sccm of this mixture was introduced into the growth chamber. Semi-insulating epi-ready GaAs and n-type InAs substrates were used for each growth.

AlSb samples 1-2 μm thick were grown at 500 to 600 ° C at either 76 torr or 200 torr with V/III ratios between 1.1 to 16. The best morphology was achieved at V/III = 15 and was independent of reactor pressure. The surface morphology of each layer was characterized by optical microscopy using Normarski interference contrast. Under this growth condition, the growth rate was 0.4 - 3.0 μm/hr for a group III transport rate of 1 to 7 $x10^{-5}$ moles of TMAA per minute.

$AlAs_{0.16}Sb_{0.84}$ layers 0.5 - 1 μm thick and lattice-matched to InAs were grown over a range of 500 to 600 ° C and 76 or 500 torr using a V/III ratio = 1.1 to 16 and

$[AsH_3]/([AsH_3]+[TESb]) = 0.1$ to 0.64 in the gas phase. The best morphology was achieved when grown on a previously grown buffer layer of InAs at a V/III ratio of 7.5 at 500 °C and 200 torr. The growth rate ranged between 0.35 - 2.0 μm/hr for two hour growth times.

Secondary ion mass spectroscopy (SIMS) was used to determine C and O impurity levels and dopant concentrations. The SIMS experiments were performed by Charles Evans and Associates, East, using Cs^+ ion bombardment.

Five crystal x-ray diffraction (FCXRD) of the (004) reflection was used to determine alloy composition. Layer thickness was determined using a groove technique and was cross checked by cross sectional SEM. These techniques usually agreed within a few percent.

Room temperature Hall measurements using the Van der Pauw technique were used to determine the majority carrier type and concentration of $AlAs_xSb_{1-x}$ layers grown on semi-insulating GaAs. Contacts were formed by alloying In/Sn (90:10) or In/Zn (95:5) at 300 °C to 340 °C for 20-30 seconds in an Ar/H_2 atmosphere.

Results And Discussion

The optimum growth conditions for $AlAs_xSb_{1-x}$ occurred at 500 °C and 200 torr at a growth rate of 1.0 μm/hour using a V/III ratio of 7.5 assuming a vapor pressure of 0.75 torr for EDMAA at 19.8°C and an [AsH3]/([AsH3]+[TESb]) ratio of 0.13. The best surface morphologies were obtained by using an InAs buffer layer. Lattice matched $AlAs_xSb_{1-x}$ films of high crystalline quality, as evidenced by five crystal x-ray diffraction (FCXRD) where full widths at half of the maximum intensity (FWHM) < 100 arc sec were obtained as shown in Figure 1(a). We were also able to reproducibly obtain lattice matching of $AlAs_xSb_{1-x}$ to InAs to within less than 0.015 percent. Surface roughness increased for growth rates of 2μm / hr. for the same V/III and [AsH3]/([AsH3]+[TESb]) conditions. GaAsSb cap layers were grown using similar conditions, a V/III of 6, and an

[AsH3]/([AsH3]+[TESb]) of 0.07. Hall measurements of $AlAs_{.16}Sb_{.84}$ films 1 μm thick with 200Å $GaAs_{.09}Sb_{.91}$ cap layers grown on GaAs substrates indicated background hole concentrations between 1 to $3x10^{17}$ cm^{-3}. The residual hole concentration of $GaAs_{.09}Sb_{.91}$ films on GaAs ranged between 4 to $7x10^{16}$ cm^{-3}.

The use of other than the above stated growth conditions led to several significant problems during the growth of $AlAs_xSb_{1-x}$ layers lattice matched to InAs. These included composition control and reproducibility. Growth at 600 °C resulted in a very broad x-ray peak that extended over hundreds of arc seconds with a constant intensity. The FWHM for the x-ray diffraction peaks were typically ≥ 500 arc seconds. Analysis of the x-ray spectra indicated that the large peak width was due to a variation of Sb composition that occured in the layer as it was grown. Sb was also detected by x-ray diffraction in InAs layers grown at 600°C following previous growths of AlAsSb. We suspect that evaporation of elemental Sb, which has a vapor pressure of 0.1 torr at 600°C, from deposits on the chamber wall results in the compositional drift observed in the AlAsSb layers grown at 600°C. Growth at 500°C greatly reduces this effect as evidenced by the improved x-ray diffraction spectrum in Figure 1(a) and the absence of Sb incorporation into InAs layers grown on top of AlAsSb. Growth at 70 or 500 torr yielded broader x-ray diffraction peaks (FWHM ≥ 300 arc seconds) with less reproducible lattice matching (≤ 500 arc seconds).

We have successfully doped the $AlAs_xSb_{1-x}$ layers both n- and p-type using TESn and DEZn. These results have been discussed in detail previously [4]. We achieved n-type doping levels of 2×10^{17} to 5×10^{18} cm^{-3} and p-type levels of 2×10^{16} to 1.4×10^{18} cm^{-3}.

We used SIMS and Hall measurements of undoped, Zn, or Sn doped $AlAs_xSb_{1-x}$ layers grown on InAs and GaAs to determine the levels of C and O impurities. Both C and O concentrations in the undoped samples are significantly lower than previously reported results ($\leq 10^{19}$ cm^{-3}) [5-11]. Oxygen levels measured in $AlAs_xSb_{1-x}$ layers are nominally the same regardless of doping or the addition of As. The source of the oxygen found in these materials is unknown at this time. The oxygen could be coming from contaminants in the organometallic

sources, the background O in the MOCVD reactor or SIMS chamber, or from reaction of the samples with air. The carbon level in undoped and Sn doped $AlAs_{0.16}Sb_{0.84}$ ($\leq 10^{18}$ cm^{-3}) is significantly lower than that found in AlSb ($1\text{-}2x10^{18}$ cm^{-3}). The observed carbon reduction is consistent with the well known effect of increased AsH_3 reducing the incorporation of C in AlGaAs films [12-14]. The higher level of carbon found in the Zn doped $AlAs_{0.16}Sb_{0.84}$ ($5x10^{18}$ cm^{-3}) is most likely related to the DEZn used for doping. It is suspected that the additional carbon is largely responsible for the Hall hole concentration considering the relatively low concentration of zinc measured by SIMS.

The details of the growth of the InAsSb/InAs multiple quantum well (MQW) structures on InAs have been previously published [15]. An x-ray diffraction pattern of an $InAs/InAs_{0.89}Sb_{0.11}$ MQW grown directly on an InAs substrate is shown in Figure 1b. The line shapes and number of satellites, out to n = 7, is indicative of the high quality of the MQW structures. The growth conditions used were 500 °C, 200 torr, a V/III ratio of 25 with an [AsH3]/([AsH3]+[TESb]) ratio of 0.75 and a growth rate of 0.9 μm/hour. The composition, x, of the $InAs_{1-x}Sb_x$ quantum wells could be varied between x = 0.1 and 0.2 by changing the [AsH3]/([AsH3]+[TESb]) flow ratio between 0.81 and 0.63 using these growth conditions. The composition changes can be explained by the use of a thermodynamic model as previously discussed [15]. The variation of composition with [AsH3]/([AsH3]+[TESb]) flow ratio is illustrated in figure 2. The variation of peak photoluminescence wavelength and presumably the bandgap with composition (x) for the $InAs_{1-x}Sb_x$ /InAs pseudomorphic superlattices grown on InAs is illustrated in Figure 3 from 4 to 6 μm. The long wavelength deviation of these bandgap values from those previously published may be explained by the CuPt-type ordering and phase separation found in these materials [16, 17]. Previous work has shown that the InAs/InAsSb interface band offset in these MOCVD grown materials is type I [18].

Although the independent growth of the $AlAs_xSb_{1-x}$ layers or the MQW structures gave uniform and reproducible x-ray diffraction patterns, when the MQW was grown sequentially on

top of the $AlAs_xSb_{1-x}$ only a very broad x-ray diffraction pattern was observed. When a layer of InAs was grown after a layer of lattice matched $AlAs_xSb_{1-x}$, a broad x-ray peak was observed at two theta values greater than the InAs substrate. SIMS measurements indicated the presence of Al in the InAs layer. In order to avoid the incorporation of Al into the quantum well structures, we developed a regrowth technique. Following the growth of the $AlAs_xSb_{1-x}$ layer capped with $GaAs_{1-x}Sb_x$ and a layer of InAsSb, the quartz reaction chamber was cleaned before growing the MQW structure. A second confinement layer of $AlAs_xSb_{1-x}$ could then be grown sequentially on top of the quantum wells without affecting the quality of the x-ray diffraction peaks. The highly crystalline quality of the InAsSb quantum wells is confirmed by x-ray diffraction where 7 orders of satellites are observed (Figure 1(b) and 1(c)) and in optical characterization where the photoluminescence linewidth was 12 meV at 14 K. The background doping of the InAs/InAsSb active region is n-type, $\approx 10^{15}$-10^{16} cm^{-3}.

The band alignments for the MOCVD grown, injection laser are shown in Figure 4. Following a $GaAs_{0.09}Sb_{0.91}$ buffer, a 2.5 micron thick $AlAs_{0.16}Sb_{0.84}$ cladding is grown on an n-type, InAs substrate. A 200Å, $GaAs_{0.09}Sb_{0.91}$ layer and a 100 Å In(Al)As(Sb) layer were placed in between the bottom cladding and a 10 period pseudomorphic MQW consisting of 500 Å InAs barriers and 100 Å $InAs_{0.88}Sb_{0.12}$ wells. A 2.5 μm thick $AlAs_{0.16}Sb_{0.84}$ cladding followed by a 200Å, $GaAs_{0.09}Sb_{0.91}$ contact and oxidation barrier layer is grown on top of the active region. None of the layers were intentionally doped. An (004) x-ray rocking curve for the laser structure is shown in Figure 1(c). The cladding layer is closely lattice-matched to the substrate ($\Delta a/a$ = 0.001), and the entire active region is pseudomorphic with the substrate and cladding layers.

LED and laser emission is observed for a variety of forward bias conditions. No emission is observed in reverse bias. The onset of the LED emission coincides with the energy of the InAsSb quantum well photoluminescence. Room temperature LED emission has been observed at 4 μm with ≥ 1 μW peak power (10 kHz, 50% duty-cycle). For LED operation, the cathode $AlAs_xSb_{1-x}$ cladding (A in Figure 4) is not necessary, but emission intensity is greater in LED's where the anode $AlAs_xSb_{1-x}$ layer (B in Figure 4) is thick enough to effectively block

electrons from leaving the active region. Gain-guided, stripe lasers were fabricated with Ti/Au metallizations. The facets were uncoated. Under pulsed operation, lasing was observed in forward bias with 40x1000 or 80x1000 micron stripes. No emission occurred under reverse bias. Devices were tested with 100 nsec pulse widths at 10 kHz (0.1 % duty-cycle). Several longitudinal modes were observed in the 3.8-3.9 μm range, shown in Figure 5 for 80 K and 200 K operation. Characteristic of the InAsSb lasers, laser emission was blue-shifted by ≈ 20 meV from the peak of the InAsSb quantum well photoluminescence [1]. Consistent with the selection rule for the compressively strained InAsSb quantum well electron (|1/2,±1/2>) -hole (|3/2,±3/2>) transition, laser emission was 100% TE polarized. The lasers displayed a sharp threshold current characteristic, and lasing was observed through 210 K as illustrated in Figure 6(a). Under pulsed operation, peak power levels ≥ 1 mW/facet could be obtained. A characteristic temperature (T_0) in the 30-40 K range was observed as shown in Figure 6(b), with the lower value (30 K) being misleading due to degradation of the device at higher temperatures.

These maximum operating temperature and characteristic temperature values are comparable to the highest values reported to date, for injection lasers of this wavelength with either strained InAsSb or InAs/GaInSb active regions [1,2,19,20]. Previously, a bipolar laser with a similar, pseudomorphic InAsSb multiple quantum well active region displayed the same characteristic temperature [1]. We believe that the characteristic temperature of both devices is limited by design of the active region and the resulting Auger rates [1]. Unlike bipolar lasers, cw operation of the unipolar laser has not yet been observed. At threshold and 100K, we find that the maximum duration of the unipolar laser output is ≈ 10^{-5} sec, with a comparable recovery time. If the device is driven above threshold with long pulses, lasing ceases and a different, low intensity emission spectrum is observed which indicates extreme band bending and depletion of the semi-metal. Examining the semi-metal device operated cw as an LED, we find that LED

emission saturates at current densities ≥ 50 A/cm^2. Due to capacitive charging within the device, the threshold current of the semi-metal laser was 10x that reported previously for the psuedomorphic, bipolar laser. Lasing pulse duration, duty-cycle, threshold current, and turn-on voltage of the semi-metal emitters may be improved with modifications in doping and heterojunction design. Further details on emitter characteristics will be presented in subsequent papers.

The use of an internal electron source enables us to consider alternative laser and LED designs that would not be feasible with conventional, bipolar devices. To our knowledge, the only comparable devices are tandem solar cells where tunnel junctions are used to internally generate electrons and holes between stages. Similarly, we can operate several stages of these semi-metal devices in series to produce multi-color LED's or increase the gain of lasers. As a demonstration, we have grown a 2-stage/ 2-color LED using InAsSb quantum wells with 11% and 13% Sb in each stage. The output of the 2-stage LED and a concurrently grown single stage LED are shown in Figure 7 along with the photoluminescence spectrum of the 2-stage LED. (Each stage is the segment A-B in Figure 4. A 600Å thick $AlAs_xSb_{1-x}$ electron barrier is placed between the 2 stages.) Low temperature emission spectra from a 2-stage LED and a 1-stage LED (grown during the same run and removed from growth chamber in the middle of the run) showed two peaks (Figure 7), corresponding to emission from each stage for the 2-stage device. Also, the relative intensities of the peaks of the 2-stage device are comparable to those observed in photoluminescence (Figure 7) which indicates that electrons are independently generated in each stage.

In conclusion, we have grown AlSb and $AlAs_xSb_{1-x}$ epitaxial layers by metal-organic chemical vapor deposition (MOCVD) using trimethylamine alane or ethyldimethylamine alane, triethylantimony, and arsine. These layers were successfully doped p- or n-type using diethylzinc or tetraethyltin, respectively. We have demonstrated the growth of high quality $AlAs_xSb_{1-x}$ by MOCVD and used it for optical confinement layers in a 3.8-3.9 μm injection laser with a novel GaSb/InAs semi-metal electron injector. The use of the InAs/GaSb semi-metal for

carrier injection, and the compatibility of the semi-metal with InAsSb devices is unique. The laser operated under pulsed conditions up to 210K with a T_o of 30-40K. These operating characteristics are comparable to the best values reported for other injection lasers operating at this wavelength. We have also reported a 2-color LED to demonstrate multi-stage operation of these devices.

Acknowledgments

We wish to thank J. A. Bur and J. H. Burkhart who provided technical assistance. This work was performed at Sandia National Laboratories, supported by the U. S. Department of Energy under contract No. DE-AC04-94AL85000

References

[1] S. R. Kurtz, R. M. Biefeld, A. J. Howard, M. H. Crawford, and M. W. Pelczynski, Appl. Phys. Lett. 68, 1332 (1996).

[2] H. K. Choi and G. W. Turner, Appl. Phys. Lett. 67, 332 (1995).

[3] Y-H. Zhang, Appl. Phys. Lett. 66, 118 (1995).

[4] R. M. Biefeld, A. A. Allerman, and M. W. Pelczynski, Appl. Phys. Lett. 68, 932 (1996).

[5] W. K. Chen, J. Ou, and W-I. Lee, Jpn, J. Appl. Phys. 33, L402 (1994).

[6] D. S. Cao, Z. M. Fang, and G. B. Stringfellow, J. Crystal Growth, 113, 441 (1991).

[7] G. J. Bougnot, A. F. Foucaran, M. Marjan, D. Etienne, J. Bougnot, F. M. H. Delannoy, and F. M. Roumanille, J. Crystal Growth, 77, 400 (1987).

[8] M. Leroux, A. Tromson-Carli, P. Gibart, C. Verie, C. Bernard, and M. C. Schouler, , J. Crystal Growth, 48, 367 (1980).

[9] C. A. Wang, M. C. Finn, S. Salim, K. F. Jensen, and A. C. Jones, Appl. Phys. Lett. 67, 1384 (1995).

[10] C. A. Wang, K. F. Jensen, A. C. Jones, and H. K. Choi, Appl. Phys. Lett. 68, 400 (1996).

[11] E. T. R. Chidley, S. K. Haywood, R. E. Mallard, N. J. Mason, R. J. Nicholas, P. J. Walker, and R. J. Warburton, J. Crystal Growth, 93, 70 (1988).

[12] G. B. Stringfellow, "Organometallic Vapor Phase Epitaxy:Theory and Practice" (Academic Press, Inc., San Diego, CA, 1989).

[13] M. A. Tischler, R. M. Potemski, T. F. Kuech, F. Cardone, M. S. Goorsky, and G. Scilla, J. Crystal Growth, 107, 268 (1991).

[14] W. S. Hobson, T. D. Harris, C. R. Abernathy, and S. J. Pearton, Appl. Phys. Lett., 58, 77 (1991).

[15] R. M. Biefeld, K. C. Baucom, and S. R. Kurtz, J. Crystal Growth, 137, 231 (1994).

[16] D. M. Follstaedt, R. M. Biefeld, S. R. Kurtz, and K. C. Baucom, J. Electronic Mater. 24, 819 (1995).

[17] S. R. Kurtz, L. R. Dawson, R. M. Biefeld, D. M. Follstaedt, and B. L. Doyle, Phys. Rev. B, 46, 1909 (1992).

[18] S. R. Kurtz, R. M. Biefeld, and A. J. Howard, Appl. Phys. Lett., 67, 3331 (1995).

[19] A. A. Allerman, R. M. Biefeld, and S. R. Kurtz, Appl. Phys. Lett., 69, 465 (1996).

[20] . R. H. Miles (private communication).

Figure Captions

Figure 1. FCXRD spectra of (a) 2.5 μm of AlAsSb latticed matched to InAs, (b) a 10 period pseudomorphic InAsSb/InAs quantum well active region grown on 2.5 μm of AlAsSb and (c) the complete electrical injection laser structure with 5 μm of AlAsSb and a 10 period MQW active region.

Figure 2. The variation of composition (x) for the $InAs_{1-x}Sb_x$ (85 Å) /InAs (425 Å) pseudomorphic superlattices grown on InAs with the vapor phase ratio of AsH_3 to AsH_3 + TESb.

Figure 3. The variation of peak photoluminescence wavelength with composition (x) for the $InAs_{1-x}Sb_x$ (85 Å) /InAs (425 Å) pseudomorphic superlattices grown on InAs.

Figure 4. Heterojunction band alignments for the MOCVD-grown, semi-metal electron injection laser. Multiple stages are possible by repeating the injector/active region cell illustrated between A and B. The polarity indicated is the forward biased condition.

Figure 5. Laser emission spectra at 1.1 x_{Ith} for (a) 80K and (b) 200K.

Figure 6. (a) Pulsed laser emission intensity versus current for various temperatures. (b) Pulsed threshold current density versus temperature. The stripe dimensions were 40x1000 μm.

Figure 7. Low temperature (14 K) LED emission spectra of a 2 stage and a 1 stage device incorporating semi-metal, injector active regions. Also shown is the photoluminescence spectra for the 2 stage device. The CO_2 feature is absent from these spectra due to nitrogen purging of the experiment.

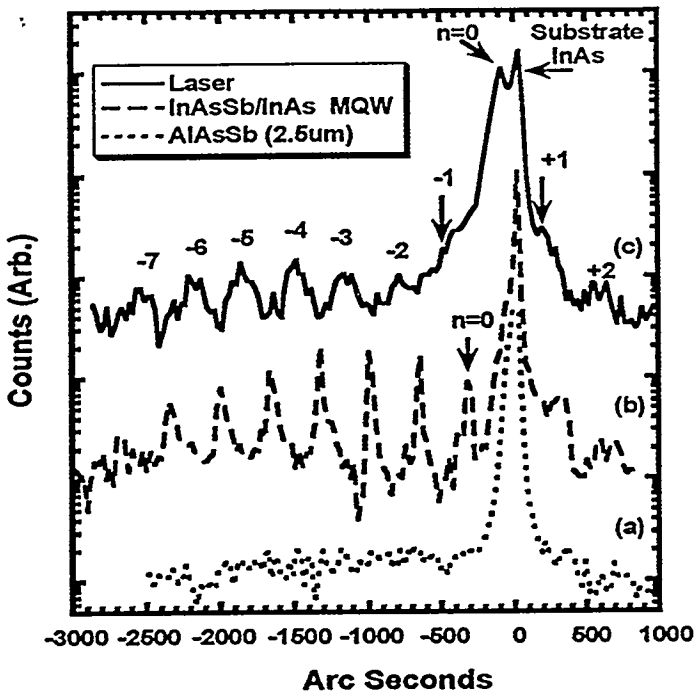

Figure 1. FCXRD spectra of (a) 2.5 μm of AlAsSb latticed matched to InAs and (b) a 10 period pseudomorphic InAsSb/InAs quantum well active region grown on 2.5 μm of AlAsSb.

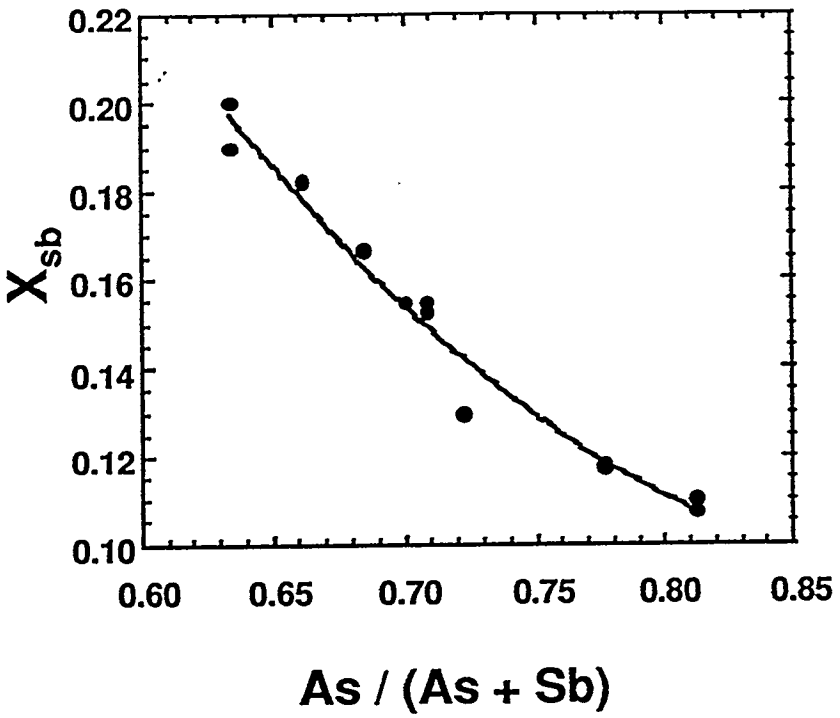

Figure 2. The variation of composition (x) for the $InAs_{1-x}Sb_x$ /InAs pseudomorphic superlattices grown on InAs with the vapor phase ratio of AsH_3 to AsH_3 + TESb.

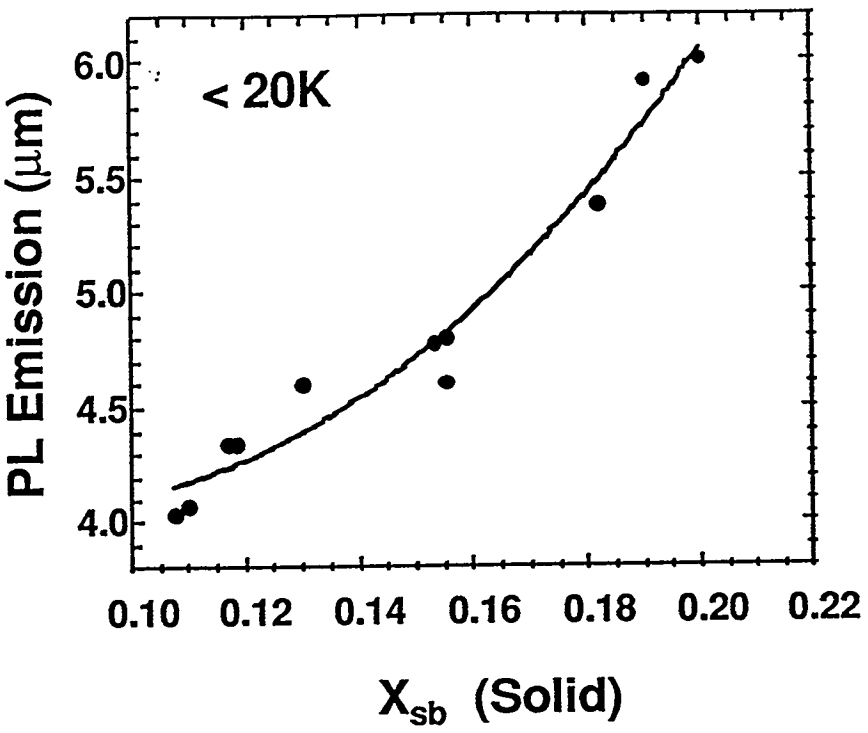

Figure 3. The variation of peak photoluminescence wavelength with composition (x) for the $InAs_{1-x}Sb_x$ /InAs pseudomorphic superlattices grown on InAs.

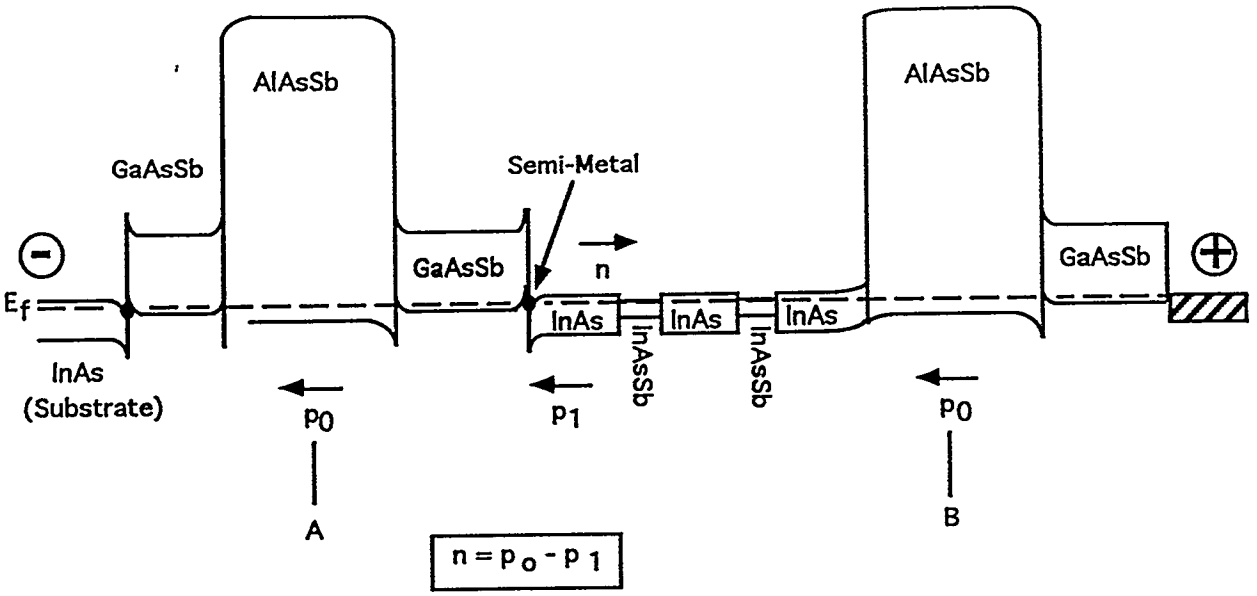

Figure 4. Heterojunction band alignments for the MOCVD-grown, semi-metal electron injection laser. Multiple stages are possible by repeating the injector/active region cell illustrated between A and B.

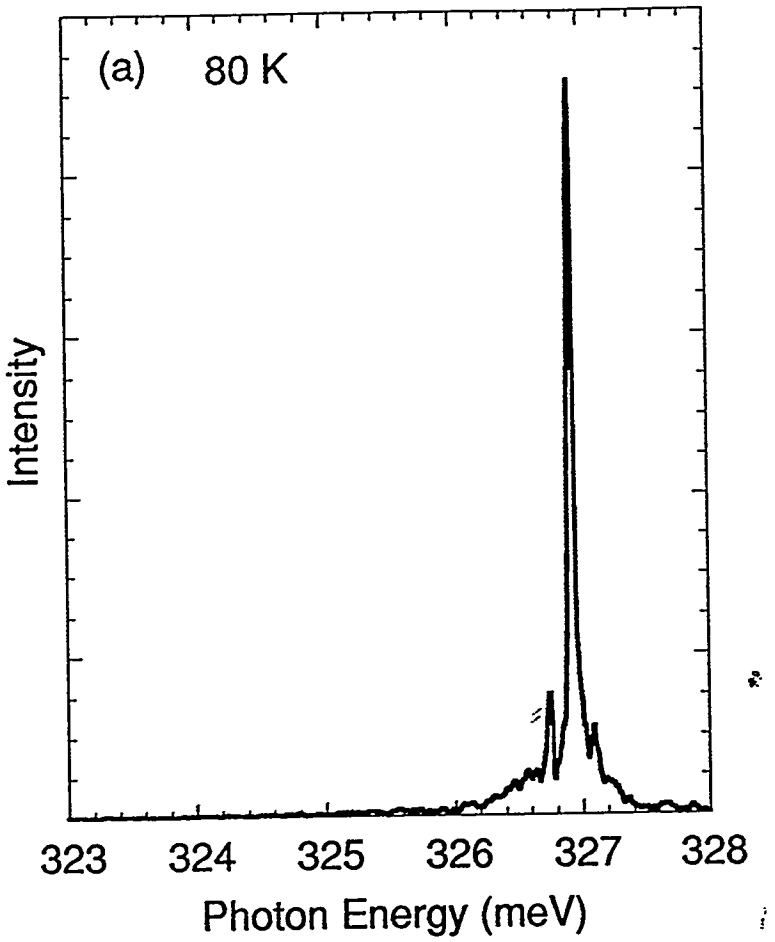

Figure 5. - Laser emission spectra at $1.1xI_{th}$ for (a) 80K

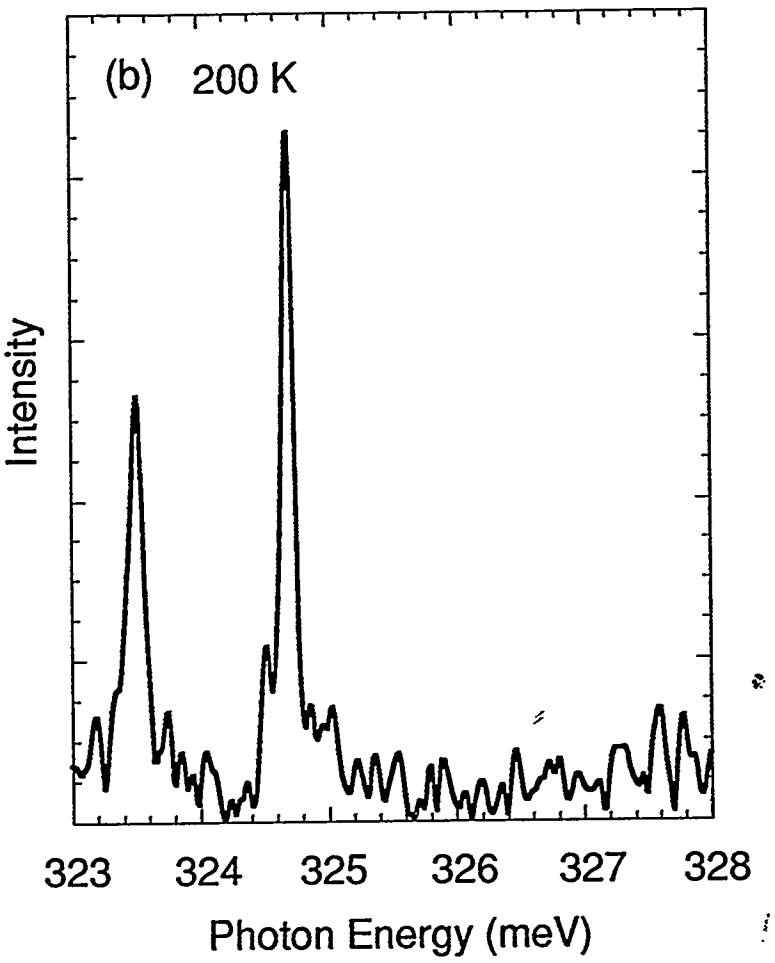

Figure 5. - Laser emission spectra at $1.1xI_{th}$ for (a) 80K and (b) 200K.

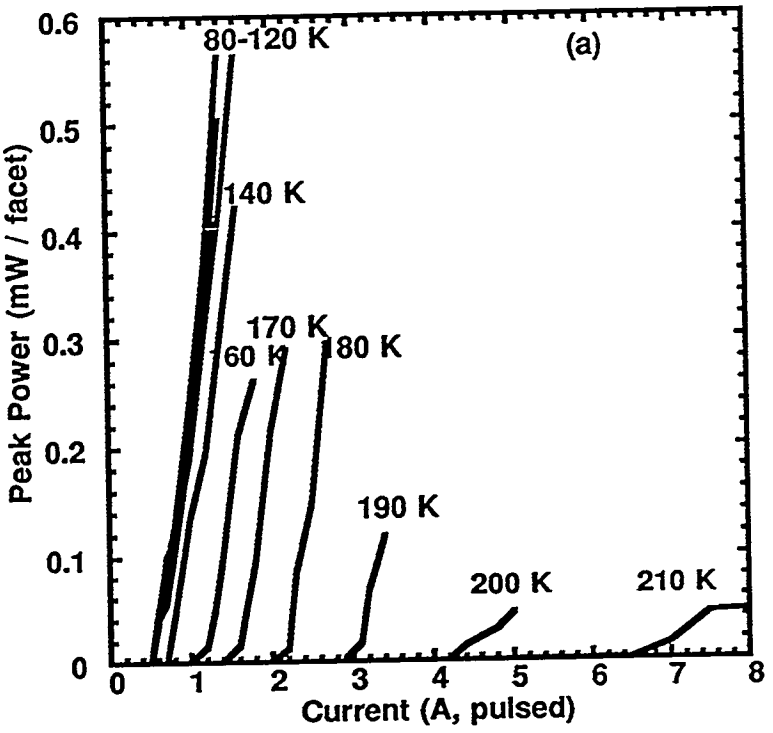

Figure 6. (a) Pulsed laser emission intensity versus current for various temperatures.

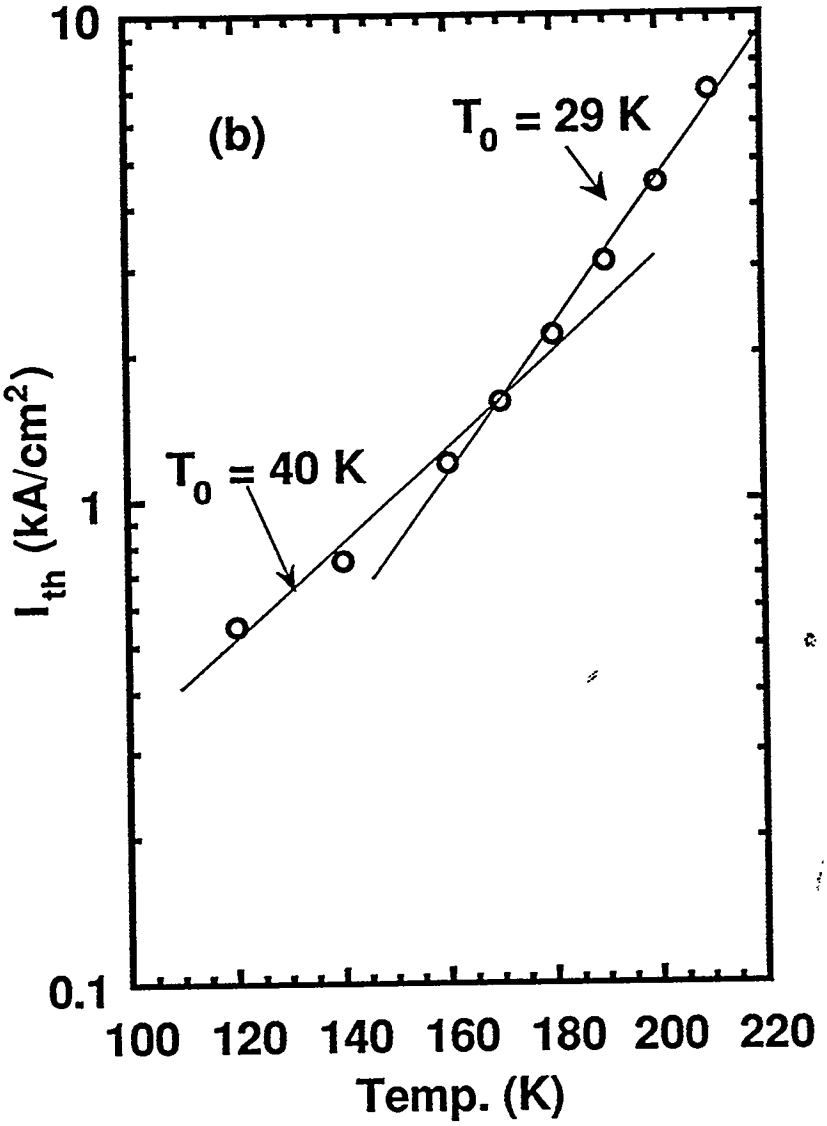

Figure 6 - (b) Pulsed threshold current density versus temperature. The stripe dimensions were 40x1000 μm.

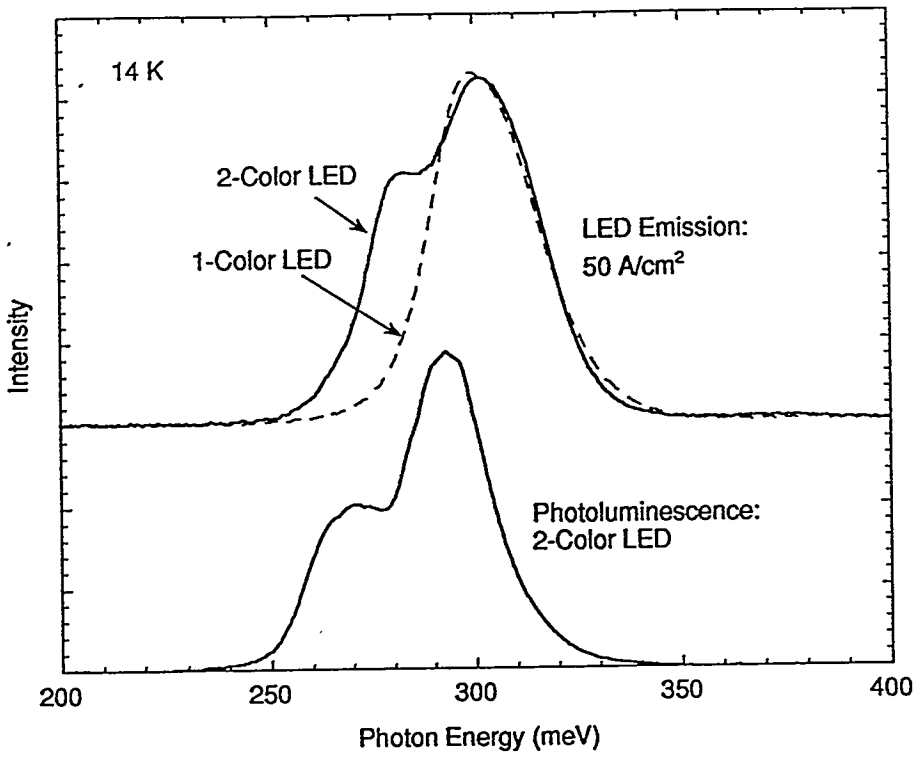

Figure 7. High resolution (14 K) LED emission spectra of a 2 stage and a 1 stage device incorporating semi- metal, injector active regions. Also shown is the photoluminescence spectra for the 2 stage device. The CO_2 feature is absent from these spectra due to nitrogen purging of the experiment.